Title

The frequency-dependent response of single aerosol particles to vapour phase oscillations and its application in measuring diffusion coefficients

Journal

Physical Chemistry Chemical Physics, 19(5)

ISSN

0956-5000

Authors

Preston, Thomas C
Davies, James F
Wilson, Kevin R

Publication Date

2017-02-01

DOI

10.1039/c6cp07711k

Peer reviewed

The Frequency-Dependent Response of Single Aerosol Particles to Vapour Phase Oscillations and its Application in Measuring Diffusion Coefficients

December 18, 2016

Thomas C. Preston,*[a] James F. Davies,[b] and Kevin R. Wilson[b]

[a] *Department of Atmospheric and Oceanic Sciences and Department of Chemistry, McGill University, 805 Sherbrooke Street West, Montreal, QC, Canada H3A 0B9*

[b] *Chemical Sciences Division, Lawrence Berkeley National Laboratory, 1 Cyclotron Road, Berkeley, California 94611, United States*

submitted to Phys. Chem. Chem. Phys.

10 Figures and 17 manuscript pages

* Thomas C. Preston

e-mail: thomas.preston@mcgill.ca

Abstract

A new method for measuring diffusion in the condensed phase of single aerosol particles is proposed and demonstrated. The technique is based on the frequency-dependent response of a binary particle to oscillations in the vapour phase of one of its chemical components. We discuss how this physical situation allows for what would typically be a non-linear boundary value problem to be approximately reduced to a linear boundary value problem. For the case of aqueous aerosol particles, we investigate the accuracy of the closed-form analytical solution to this linear problem through a comparison with the numerical solution of the full problem. Then, using experimentally measured whispering gallery modes to track the frequency-dependent response of aqueous particles to relative humidity oscillations, we determine diffusion coefficients as a function of water activity. The measured diffusion coefficients are compared to previously reported values found using the two common experiments: (i) the analysis of the sorption/desorption of water from a particle after a step-wise change to the surrounding relative humidity and (ii) the isotopic exchange of water between a particle and the vapour phase. The technique presented here has two main strengths: First, when compared to the sorption/desorption experiment, it does not require the numerical evaluation of a boundary value problem during the fitting process as a closed-form expression is available. Second, when compared to the isotope exchange experiment, it does not require the use of labeled molecules. Therefore, the frequency-dependent experiment retains the advantages of these two commonly used methods but does not suffer from their drawbacks.

1 Introduction

Secondary organic aerosol (SOA) particles, formed after volatile organic compounds are oxidized and condense,[1–7] can be highly viscous under a wide range of atmospheric conditions.[8–11] The high viscosity condensed phase of the SOA slows mass transfer due to low diffusivity. Characteristic equilibration times associated with diffusion will be much larger in a high viscosity SOA particle than in a liquid-phase particle.[12] This can influence reactive uptake[13–16] and greatly diminish the rate of water sorption and desorption.[17,18]

Accurate measurements of water diffusivity in SOA are key to modelling gas-particle partitioning and understanding mass transport in the particle phase of atmospheric aerosols. Laboratory based, single particle techniques allow measurements with low uncertainties due to the absence of distributions in size and composition that will be present in an ensemble of aerosol particles.[19–25] For studies of SOA in the lab, binary systems consisting of water and a surrogate for the oxygenated organic material found in an SOA are often examined due to ease of preparation and the availability of tabulations of physical parameters for such aqueous systems (e.g. sucrose is commonly used). However, even in a model system, determining water diffusivity across an atmospherically relevant range of temperature and relative humidity (RH) can be challenging. First, small diffusivity that occurs at low temperature and/or low RH can result in experimental timescales of days.[17,26–28] Second, the retrieval of diffusion coefficients through the analysis of measured data sets is not always easy. In the common sorption/desorption experiment, the response of a particle to a step-wise change in RH is measured. Analyzing this response is complicated and time consuming as the mathematical model (a non-linear boundary value problem) needs to be evaluated numerically.[17]

An alternative to the sorption/desorption experiment is the isotope exchange experiment.[29–31] A particle is first equilibrated at the RH of interest using vapour that is pure H_2O. Then, while maintaining the same RH, the vapour source is changed to pure D_2O. The uptake of D_2O (and loss of H_2O) by the particle is easily tracked using Raman spectroscopy and the diffusion coefficient can be determined from the change in the intensity of the scattered Raman light over time. Analyzing the measurements does not involve the same mathematical complexity as the sorption/desorption experiment due to the constant RH.[32] The size of the particle remains approximately constant so there is no moving boundary. Additionally, the activity of water is uniform throughout the particle so the diffusion coefficient is constant (there are gradients in the concentrations of H_2O and D_2O but not in overall amount of water). Finally, the non-linear boundary condition that exists at the surface of the particle for the sorption/desorption experiment is linear for the model that describes the isotope exchange experiment as the concentration of water at the surface does not change. All of these simplifications yield a linear boundary value problem that can be solved analytically. The closed-form solution to the diffusion problem makes the analysis of measurements much more straightforward compared to the sorption/desorption experiments.

Despite the simplifications that the isotope exchange experiment introduces to the analysis of measurements, it currently cannot be thought of as a replacement for the sorption/desorption experiment. This is because large discrepancies (in some cases orders of magnitude) between diffusion coefficients retrieved using the two experiments have been reported.[31,33] As of now there is no satisfactory explanation as to the origin of these discrepancies and the preferred use of results from the sorption/desorption experiment has been justified on the basis that the experiment provides a closer representation of actual atmospheric processes.[33]

In this work, we propose and demonstrate a new method to measure diffusion coefficients in binary particles containing a volatile and a non-volatile component. The method relies on measuring the frequency-dependent response (e.g. change in radius) of a particle to oscillations of one of its chemical components in the vapour phase. Approximate analytical solutions to this non-linear boundary value problem are found and discussed (Section 2). Then, the accuracy of these solutions are assessed through a comparison to numerical simulations for an aqueous sucrose particle as the RH oscillates at different frequencies (Section 3). Through the use of simulations and experiments, it is shown that shifts in whispering gallery modes modes (WGMs) are sensitive enough to track the response of a particle to very small RH oscillations (Sections 4 and 5). The closed-form expression for the amplitude of the oscillations is then used to analyze measurements from both aqueous sucrose and citric acid particles (Section 5). This analysis involves both the retrieval of diffusion coefficients from frequency-dependent measurements and a comparison to previous parameterizations of diffusivity.

2 Theory

2.1 Overview

We will develop a mathematical model that describes the time-dependent change in the radius of a particle containing two chemical components as the vapour phase concentration of one component varies (e.g. by changing the RH if one component is water). We will focus on the specific case where the variations in vapour phase concentration are small and vary sinusoidally over time. Furthermore, we will assume that one component of the particle is non-volatile. Section 2.2 outlines the boundary value problem and Section 2.3 provides an analytical solution

to the problem of determining the concentration profile inside the particle while vapour phase oscillations take place. Finally, in Section 2.4 the solution from Section 2.3 is used to determine the time-dependent radius of the particle.

2.2 Statement of the problem

For a binary system containing species A and B with mass concentrations ρ_A and ρ_B, velocities $\mathbf{v}_A$ and $\mathbf{v}_B$, and mass fractions w_A and w_B the convection-diffusion equation for A is[34]

$$\frac{\partial \rho_A}{\partial t} + \nabla \cdot (\rho_A \mathbf{v}) = \nabla \cdot (\rho D \nabla w_A) \tag{1}$$

and the continuity equation is

$$\frac{\partial \rho}{\partial t} + \nabla \cdot (\rho \mathbf{v}) = 0, \tag{2}$$

where ρ is the mass density of solution, $\rho = \rho_A + \rho_B$, D is the concentration-dependent diffusion coefficient, and $\mathbf{v}$ is the mass average velocity, $\mathbf{v} = w_A \mathbf{v}_A + w_B \mathbf{v}_B$. We have used the Fickian formulation of mass transfer where the non-ideality of the system is incorporated into D.[35] If the problem had been formulated using molar units, D would be identical.

For a spherical particle with a time-dependent radius, $s(t)$, and a mass concentration that only depends on r and t (spherical symmetry) the model is

$$\frac{\partial \rho_A}{\partial t} + \frac{1}{r^2}\frac{\partial}{\partial r}(r^2 v_r \rho_A) = \frac{1}{r^2}\frac{\partial}{\partial r}\left(r^2 \rho D \frac{\partial w_A}{\partial r}\right) \quad \text{for} \quad 0 < r < s, \quad t > 0, \tag{3}$$

$$\frac{\partial \rho}{\partial t} + \frac{1}{r^2}\frac{\partial}{\partial r}(r^2 \rho v_r) = 0 \quad \text{for} \quad 0 < r < s, \quad t > 0, \tag{4}$$

where v_r is the radial component of $\mathbf{v}$.

For a particle where $s(0) = s_0$, the initial conditions are

$$\rho_A = \rho_{A_0} \quad \text{and} \quad v_r = 0 \quad \text{for} \quad r \leq s_0, \quad t = 0. \tag{5}$$

Symmetry can be used to find the two boundary conditions

$$\frac{\partial \rho_A}{\partial r} = 0 \quad \text{and} \quad v_r = 0 \quad \text{at} \quad r = 0, \quad t > 0. \tag{6}$$

A third boundary condition can be found by assuming that the time-dependent mass concentration of A outside of the particle, $\rho_A^v(t)$, is uniform across r and, at that the surface of the particle, ρ_A is in equilibrium with this concentration. This gives

$$\rho_A = \frac{RT_s\rho_s}{\gamma p_0 M_s}\rho_A^v \quad \text{at} \quad r = s, \quad t > 0, \tag{7}$$

where γ is the activity coefficient of A for w_A at $r = s$, p_0 is the vapour pressure of A, R is the gas constant, T_s is the temperature, M_s is the average molar mass of the solution at $r = s$, and ρ_s is the mass density of the solution at $r = s$. The effect of surface curvature has been ignored. For brevity, we will write the boundary condition in Eq. 7 as $\rho_A = \beta(t)$ at $r = s$ when discussing it in the following sections.

The final boundary condition can be found by first examining the mass conservation of B across the surface of the particle:

$$(\rho_B^v - \rho_B)\frac{ds}{dt} = j_{B,r}^v - j_{B,r} + \rho_B^v v_r^v - \rho_B v_r \quad \text{at} \quad r = s, \quad t > 0, \tag{8}$$

where ρ_B^v is mass concentration of B outside of the particle (in the vapour phase), $j_{B,r}$ and $j_{B,r}^v$ are the mass fluxes inside and outside of the particle, respectively, and v_r^v is the mass average velocity outside of the sphere. Eq. 8 can be reduced as follows:[36] First, assume that B is non-volatile. This allows one to set $\rho_B^v = 0$ and $j_{B,r}^v = 0$ for $r > s$. Second, insert the relationship $j_{B,r} = -j_{A,r}$ into the equation and apply the definition $j_{A,r} = -\rho D \nabla w_A$. Then, after some manipulation, Eq. 8 can be rewritten as

$$\frac{ds}{dt} = v_r + \frac{D}{1 - w_A}\nabla w_A \quad \text{at} \quad r = s, \quad t > 0. \tag{9}$$

2.3 Solution to the boundary value problem

The boundary value problem of interest is defined by Eqs. 3, 4, 5, 6, 7, and 9. For the experiment discussed in Section 2.1, we define $\beta(t)$ as

$$\beta(t) = \rho_{A_0} + \epsilon \sin \omega t, \tag{10}$$

where ω and ϵ are the angular frequency and amplitude of the oscillations of the mass concentration of A in the particle phase at $r = s$, respectively. In the following analysis we will assume that the oscillations of A in the vapour phase are small and, therefore, $\epsilon \ll \rho_{A_0}$. Consequently, we will only be dealing with small changes in ρ and we will assume that the equilibrium mass density ρ_{eq} is a linear function of ρ_A:

$$\frac{\rho_{eq}}{\rho_0} = 1 + \alpha(\rho_A - \rho_{A_0}), \tag{11}$$

where ρ_0 is the mass density of solution when $\rho_A = \rho_{A_0}$. Furthermore, because the variation of ρ with r is small we will also assume that $\nabla \cdot (\rho D \nabla w_A) \approx \nabla \cdot (D \nabla \rho_A)$.

Setting $\rho_{eq} = \rho$ in Eq. 11 and inserting the result into Eq. 4 gives an equation that can be combined with Eq. 3 and integrated using the boundary condition in Eq. 6 to obtain

$$v_r = \frac{\alpha D}{\alpha \rho_{A_0} - 1} \frac{\partial \rho_A}{\partial r}. \tag{12}$$

With Eq. 12, v_r can be eliminated from Eq. 3 to yield

$$\frac{\partial \rho_A}{\partial t} = \frac{1}{r^2} \frac{\partial}{\partial r} \left(r^2 D_c \frac{\partial \rho_A}{\partial r} \right), \tag{13}$$

where

$$D_c = D \left(1 - \frac{\alpha \rho_A}{\alpha \rho_{A_0} - 1} \right).$$

Again, because $\epsilon \ll \rho_{A_0}$, both D_c and $s(t)$ will be approximately constant. Therefore, we can form the following linear boundary value problem from Eqs. 5, 6, 7, and 13:

$$\frac{\partial \rho_A}{\partial t} = \frac{D_c}{r^2}\frac{\partial}{\partial r}\left(r^2 \frac{\partial \rho_A}{\partial r}\right) \quad \text{for} \quad 0 < r < s_0, \quad t > 0, \tag{14}$$

$$\rho_A = \rho_{A_0} + \epsilon \sin \omega t \quad \text{at} \quad r = s_0, \quad t > 0, \tag{15}$$

$$\frac{\partial \rho_A}{\partial r} = 0 \quad \text{at} \quad r = 0, \quad t > 0, \tag{16}$$

$$\rho_A = \rho_{A_0} \quad \text{for} \quad r \leq s_0, \quad t = 0. \tag{17}$$

where ρ_A in D_c is set equal to ρ_{A_0}. An analytical solution to this problem can be found using the method of eigenfunction expansion:

$$\rho_A(r,t) = \rho_{A_0} + \epsilon \sin \omega t + \sum_{n=1}^{\infty} \frac{2 s_0^3 (-1)^n \omega \epsilon}{r(\pi^5 n^5 D_c^2 + \pi n s_0^4 \omega^2)} \sin\left(\frac{\pi n r}{s_0}\right) \Big(\pi^2 n^2 D_c \cos \omega t + s_0^2 \omega \sin \omega t - \pi^2 n^2 D_c e^{-\pi^2 n^2 D_c t / s_0^2}\Big). \tag{18}$$

Using the dimensionless variables

$$\tilde{r} = \frac{r}{s_0}, \quad \tilde{\omega} = \frac{s_0^2 \omega}{D_c}, \quad \tilde{t} = \frac{D_c t}{s_0^2}, \quad \tilde{\rho}_A = \frac{\rho_A}{\rho_{A_0}}, \quad \text{and} \quad \tilde{\epsilon} = \frac{\epsilon}{\rho_{A_0}},$$

Eq. 18 can be rewritten as

$$\tilde{\rho}_A(\tilde{r}, \tilde{t}) = 1 + \tilde{\epsilon} \sin \tilde{\omega} \tilde{t} + \frac{2\tilde{\omega}\tilde{\epsilon}}{\tilde{r}} \sum_{n=1}^{\infty} \frac{(-1)^n \sin \pi n \tilde{r}}{\pi^5 n^5 + \pi n \tilde{\omega}^2} \left(\pi^2 n^2 \cos \tilde{\omega} \tilde{t} + \tilde{\omega} \sin \tilde{\omega} \tilde{t} - \pi^2 n^2 e^{-\pi^2 n^2 \tilde{t}}\right). \tag{19}$$

Fig. 1 shows $\tilde{\rho}_A$ as a function of $\tilde{r}$ at various $\tilde{t}$ and $\tilde{\omega}$. When $\tilde{\omega}$ is very small, the spherical particle will essentially equilibrate with the vapour at any $\tilde{t}$ and $\tilde{\rho}_A$ will be nearly constant across $\tilde{r}$. As $\tilde{\omega}$ increases, larger gradients in $\tilde{\rho}_A$ occur. These gradients are strongest near the surface ($\tilde{r} = 1$) and decrease when moving towards the particle centre ($\tilde{r} = 0$). This inner-surface localization of the gradients becomes more pronounced with increasing $\tilde{\omega}$. Eventually, at very large $\tilde{\omega}$, $\tilde{\rho}_A \simeq 1$ everywhere except at $\tilde{r} = 1$.

2.4 Time-dependent radius

To determine $s(t)$, we first insert Eq. 12 into Eq. 9 and apply the approximations discussed earlier. This yields

$$\frac{ds}{dt} = D_s \frac{\partial \rho_A}{\partial r} \quad \text{at} \quad r = s_0 \quad \text{for} \quad t > 0, \tag{20}$$

where

$$D_s = D\left(\frac{\alpha}{\alpha\rho_{A_0} - 1} + \frac{1}{\rho_0 - \rho_{A_0}}\right). \tag{21}$$

Then, inserting Eq. 18 into 20 and integrating with respect to time gives

$$s(t) = s_0 + 2s_0\epsilon D_s \sum_{n=1}^{\infty} \frac{s_0^2\omega e^{-\pi^2 n^2 D_c t/s_0^2} + \pi^2 n^2 D_c \sin\omega t - s_0^2\omega\cos\omega t}{\pi^4 n^4 D_c^2 + s_0^4\omega^2}. \tag{22}$$

Using various trigonometric relationships and evaluating the infinite series that are products with the sin and cos functions in Eq. 22 yields

$$s(t) = s_0 + C\sin(\omega t + \theta) + 2s_0\epsilon D_s \sum_{n=1}^{\infty} \frac{s_0^2\omega e^{-\pi^2 n^2 D_c t/s_0^2}}{\pi^4 n^4 D_c^2 + s_0^4\omega^2}, \tag{23}$$

where

$$C = \frac{D_s\epsilon}{\omega s_0}\sqrt{(\mu\cot\mu - 1)(\mu\coth\mu - 1)}, \tag{24}$$

$$\tan\theta = \frac{2i/\mu - i\cot\mu + \cot i\mu}{i\cot i\mu - \cot\mu}, \tag{25}$$

and

$$\mu^2 = i\frac{s_0^2\omega}{D_c}. \tag{26}$$

For large values of t, the last term in Eq. 23 will be negligible and

$$s(t) = s_0 + C\sin(\omega t + \theta). \tag{27}$$

It is clear from Eq. 27 that the phase difference between the oscillations of $s(t)$ and $\beta(t)$ is θ and that these oscillations occur with an amplitude C (when $\beta(t)$ is defined using Eq. 10). It is also

convenient that such a relatively simple expression like Eq. 27 can describe the steady-state oscillations of $s(t)$.

Fig. 2 shows $\tilde{C}$ and θ as a function of $\tilde{\omega}$, where $\tilde{C} = CD_c/(D_s \epsilon s_0)$ (the dimensionless amplitude). Both S-shaped curves have plateaus outside of the region between $\tilde{\omega} \simeq 1$ and $\tilde{\omega} \simeq 10^5$. As $\tilde{\omega}$ goes to zero, θ goes to zero and $\tilde{C}$ approaches its maximum value. As $\tilde{\omega}$ goes to infinity, θ goes to its minimum value of $-\pi/4$ and $\tilde{C}$ goes to zero.

3 Comparison between numerical and analytical results for an aqueous particle

In this section we apply the theory developed in Section 2 to systems where species A is water and $\beta(t)$ is related to the time-dependent RH oscillations that occur in the vapour phase. As will be shown in Section 5, such systems can be studied using single aerosol particles in a laboratory using an RH controlled cell where measurements of C and/or θ at various ω allow for the retrieval of D as a function of water activity. Here, we evaluate the accuracy of the solutions found in Section 2.4 through a comparison with results found using a numerical scheme that evaluates the non-linear boundary value problem. Numerical results are calculated using the finite difference method outlined by Zobrist *et al.*[17] The binary system considered here is water and sucrose. This system is well-studied and sucrose has often been used as a surrogate for oxygenated organics found in SOA particles.[17,27,29,31,37]

Fig. 3 shows the response of an aqueous sucrose particle to RH oscillations with an amplitude of 2.5% at three different mid-point RHs. An amplitude of 2.5% was chosen as this is more than adequate to allow for the response of a particle to be monitored using WGMs (see Sections 4

and 5). The period, T, of the RH oscillations was 100 s (where $T = 2\pi/\omega$). For these examples, the analytical calculation of s was done using either Eq. 23 or 27. The only difference between these two equations is the presence of the transient term in Eq. 23. This term allows Eq. 23 to correctly determine s at $t = 0$. Also, at small t it will more closely match the numerical calculations. At longer t both analytical equations give similar results. From Fig. 3 it can be seen that s determined using Eqs. 23 and 27 is systematically lower than s found numerically. However, the accuracy of both the predicted amplitude and phase of the oscillations in s is excellent. For the corresponding panels in Fig. 3, C calculated using Eq. 24 is (a) 0.44, (b) 1.75, and (c) 12.30 nm while the amplitude from the numerical plots is (a) 0.45, (b) 1.73, and (c) 11.81 nm. Similarly, θ calculated using Eq. 25 closely matched the phase difference between the RH oscillations and s calculated numerically.

The effect of RH oscillation amplitude on accuracy is examined in Fig. 4. As the amplitude of the RH oscillations increases (Fig. 4a to d), the error between the analytical and numerical results also increases. Several approximations are made in Section 2.3 that can lead to this increasing error. Fig. 4e was generated using parameters identical to those used to generate Fig. 4d except that D was constant. This leads to a significant reduction in the error between the numerical and analytical calculations. Therefore, the assumption that D is constant with respect to ρ_A appears to rapidly become invalid with increasing RH amplitude (as oppose to the assumption of constant s or the linearization of ρ).

The above examples demonstrate the potential accuracy of the solutions presented in Section 2.4. However, only one T was considered in Figs. 3 and 4. In order to investigate the accuracy across a larger range of conditions, C and θ were calculated both analytically and numerically from $T = 10^{-1}$ to 10^{7} s for three different mid-point RHs (Fig. 5). Note that it is very time

consuming to calculate multiple values of C and θ numerically whereas when Eqs. 24 and 25 are used a curve across any range of T can be generated immediately. Overall, there is excellent agreement between the analytical and numerical calculations across this large range of T. Therefore, Eqs. 24 and 25 can be used when analyzing the response of aqueous particles to small oscillations in RH for systems with similar physical parameters to those analyzed here.

4 Tracking the response of a particle using WGMs

The response of a spherical particle to changes in the surrounding RH can be tracked using WGMs. The position of the WGMs are very sensitive to both changes in s and m (refractive index) of the sphere.[22,38] For example, Fig. 6a shows the calculated extinction efficiency, Q_{ext}, of an aqueous sucrose particle equilibrated at RH = 30%. As oscillations in RH occur, the peaks in Q_{ext} will shift as both s and the profile of m inside the particle change in response to the oscillating RH. In Fig. 6b, the peak associated with the TE^{3}_{57} mode is shown during a sinusoidal RH oscillation with T = 100 s and an amplitude of 2.5%. Although the peak only shifts several tenths of a nanometre during the RH oscillation, this type of change can readily be detected.[39] Larger amplitudes in RH oscillations will lead to larger shifts. However, as discussed in Section 3, the accuracy of the model developed here decreases with increasing RH amplitude. Experimentally one needs to balance the amplitude of RH oscillations with the observed amplitude of oscillations in the WGM resonance positions. The amplitude of RH oscillations must be large enough to give a clear signal but not so large that the model used to analyze the data will be inaccurate.

Tracking particle response using WGMs introduces the problem that one is measuring peak positions over time rather than the desired radius over time. For a homogeneous spherical

particle this is not an issue as the process of determining both s and m from WGM positions is fast and accurate.[38] Here, though, the concentration profile inside the particle is no longer uniform once the RH oscillations begin so the process of converting measured WGMs into s is not straightforward. Using a fitting algorithm for a homogeneous sphere will not give accurate results (except in the plateau regions of Fig. 2). In principle, peak positions for a sphere with a non-uniform concentration profile can be calculated using an electromagnetic scattering code for a multilayered sphere.[40] For instance, the Q_{ext} curves in the previously discussed Fig. 6b were generated using such code. However, these calculations are extremely time consuming if the concentration profile is not known beforehand (and that would be the case during the fitting process). Therefore, we will focus on the direct analysis of the oscillations in WGM positions and the information that can be extracted from these measurements.

Fig. 7 shows the amplitude of the oscillations in peak position for the TE^3_{57} mode at various T for aqueous sucrose at a mid-RH of 30%. The calculated amplitude from Eq. 24 is superimposed on these data points. The correlation between the curve and the data points is quite good. This demonstrates a straightforward method for determining D as a function of water activity: First, use the measured amplitude of mode oscillations across a range of T to create a set of measured data points. Second, fit these measurements using Eq. 24 to retrieve D for a particular mid-RH. Finally, perform a series of similar experiments where the only parameter that is altered is the mid-RH. This will allow for D to be found over a range of water activities. The tradeoffs for the simplicity of this approach are: (i) the amplitude scale is arbitrary so information about the magnitude of the oscillations is not used during the fitting process, and (ii) the phase of the oscillations cannot be directly extracted from the WGM positions. This second point is a consequence of the fact that along with s changing

during the RH oscillations so does the profile of m inside the particle. If m were uniform, phase information could be directly extracted from the WGM positions. However, as discussed earlier, the assumption of a homogeneous sphere is not satisfactory here so this is not feasible with this simple method.

5 Experimental determination of diffusivity using the response of an aerosol particle to RH oscillations

Experimental verification of the frequency-dependent method described in the earlier sections was achieved using an Aerosol Optical Tweezers (Biral AOT-100). Details on the use of optical tweezers for aerosol research have been presented in detail elsewhere[31] and are recounted only summarily here. Aqueous particles of either sucrose or citric acid were generated in a nebulizer plume and introduced into an environmentally controlled chamber where a single particle became confined at the focal point of a 532 nm laser (Laser Quantum 2W Opus) focused through a microscope objective (Olympus PLFLN 100X objective). Typical trapping powers were between 30 and 50 mW. For the equilibrated particle, s_0 was determined at a given mid-RH using the observed positions of WGM wavelengths in the Raman spectrum.[22,38] Raman spectra were acquired using a Princeton Instruments Acton SP2500i spectrometer with a grating of 1200 grooves/mm and a PIX-256E CCD. After equilibration, the RH was then varied sinusoidally with an amplitude of 2.5% by varying the ratio of wet and dry nitrogen gas flows delivered by two mass flow controllers (MKS MF-1). The total flow rate was a constant 300 sccm. The response of the particle to RH oscillations at various T and mid-RHs was monitored using the location of WGM wavelengths. During the experiment, RH was measured as a function of

time using RH probes (Honeywell HIH-4602C) that were placed before and after the trapping chamber.

Fig. 8 shows the dependence of two WGM peaks arising from an aqueous sucrose particle with $s_0 = 4630$ nm at four different T and a mid-RH of 39%. For the chosen RH amplitude of 2.5%, oscillations in WGMs are readily observed. With increasing T, the amplitude of the WGM oscillations in both mode orders shown in Fig. 8 increases and the phase difference between the RH oscillations and WGM oscillations approaches zero. In Section 4, we discussed why the analysis of phase information from WGM measurements is a challenge. To reiterate, in general, m is not uniform at any given t during the experiment so there is no straightforward way to relate the phase of WGMs to the phase of s. Therefore, we will focus on the analysis of amplitude for the remainder of this section. As discussed in Section 4, the amplitude of WGM oscillations correlates well with the amplitude of oscillations in s.

The oscillatory response was measured for both aqueous sucrose and aqueous citric acid particles for a range of T and mid-RH values. Amplitudes taken from these responses are summarized in Figs. 9 and 10 and compared to the predicted dependencies using three parameterizations of water diffusion for sucrose[17,29,31] and one for citric acid.[31] In both Figs. 9 and 10, error bars of ± 0.05 are representative of the uncertainty in the amplitude, arising from the instrument response at short time periods, the amplitude at infinite time periods, and the variability in amplitudes across all resonant modes in the Raman spectrum. Overall, the agreement between measurements taken using the frequency-dependent method and parameterizations found using the isotopic exchange experiment is good.

The phase and amplitude offset in the measured RH for high frequency oscillations arise primarily due to the time-response of the probes (with e-folding times of approximately 60 s)

and the time for the chamber to respond (on the order of 10-30 s). Calibration experiments using LiCl particles (assumed to exhibit no diffusion limitations under these conditions) confirmed that the RH cycling experienced by particles in the trap retained the same amplitude across all experimental frequencies reported. The instrument response is also shown in Fig. 10. This represents an upper limit of the amplitude that can be measured at any given T. Based on this limit and typical particle sizes, with the current setup, it is not possible to measure amplitudes for aqueous systems where D is above the order of 10^{-13} m^2/s. Therefore, the method described here is suitable for retrieving diffusion coefficients of viscous, aqueous particles.

6 Conclusion

We have found a closed-form expression that describes the response of a particle to vapour phase oscillations. Through a comparison with numerical results, the accuracy of this solution was discussed for cases where aqueous particles are exposed to oscillations in the surrounding RH and its suitability was demonstrated for RH oscillations with an amplitude of 2.5%. For aqueous particles, it was shown, through both modelling and experiment, that the measured amplitude from the response of WGMs to RH oscillations could be used to determine diffusivity across a range of water activities. This represents a new method for retrieving water diffusivity in aerosol particles. The advantages of this approach over existing methods are that it does not require the numerical evaluation of partial differential equations during the retrieval process (unlike the sorption/desorption experiment) and it does not require the use of isotopic labels (unlike D_2O/H_2O isotopic exchange experiments). Given the benefits of this experiment we are hopeful that it will find use in laboratories that study water diffusivity in high viscosity aerosol particles.

Acknowledgements

T.C.P. acknowledges support from the Natural Sciences and Engineering Research Council of Canada (NSERC). J.F.D and K.R.W. acknowledge the support of the Department of Energy's Office of Science Early Career Research Program and of the Director, Office of Energy Research, Office of Basic Energy Sciences, Chemical Sciences, Geosciences, and Biosciences Division of the U.S. Department of Energy under Contract No. DE-AC02-05CH11231.

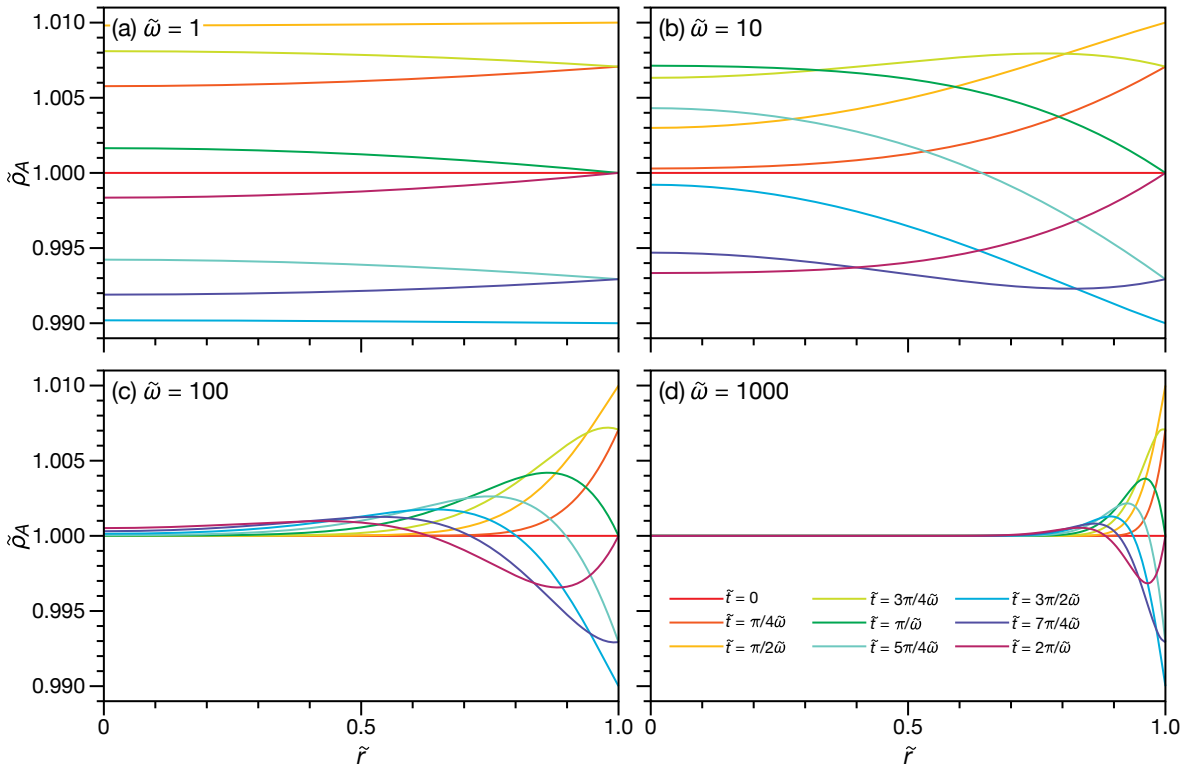

Figure 1: The dimensionless mass concentration of component A, $\tilde{\rho}_A$, as a function of the dimensionless radial coordinate, $\tilde{r}$, at various dimensionless times, $\tilde{t}$, for (a) $\tilde{\omega} = 1$, (b) $\tilde{\omega} = 10$, (c) $\tilde{\omega} = 100$, and (d) $\tilde{\omega} = 1000$, where $\tilde{\omega}$ is the dimensionless angular frequency. The values of $\tilde{t}$ are between $\tilde{t} = 0$ and $\tilde{t} = 2\pi/\tilde{\omega}$ (across one period). In all cases $\tilde{\epsilon} = 0.01$, where $\tilde{\epsilon}$ is the dimensionless amplitude of oscillation of $\tilde{\rho}_A$ at $\tilde{r} = 1$ (the particle surface).

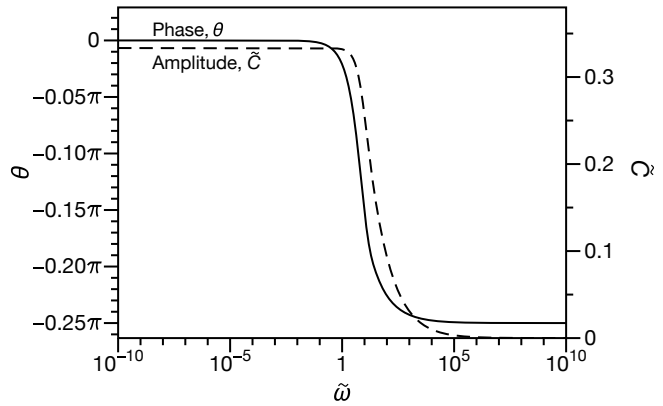

Figure 2: Phase, θ, and dimensionless amplitude, $\tilde{C}$, as a function of dimensionless angular frequency, $\tilde{\omega}$.

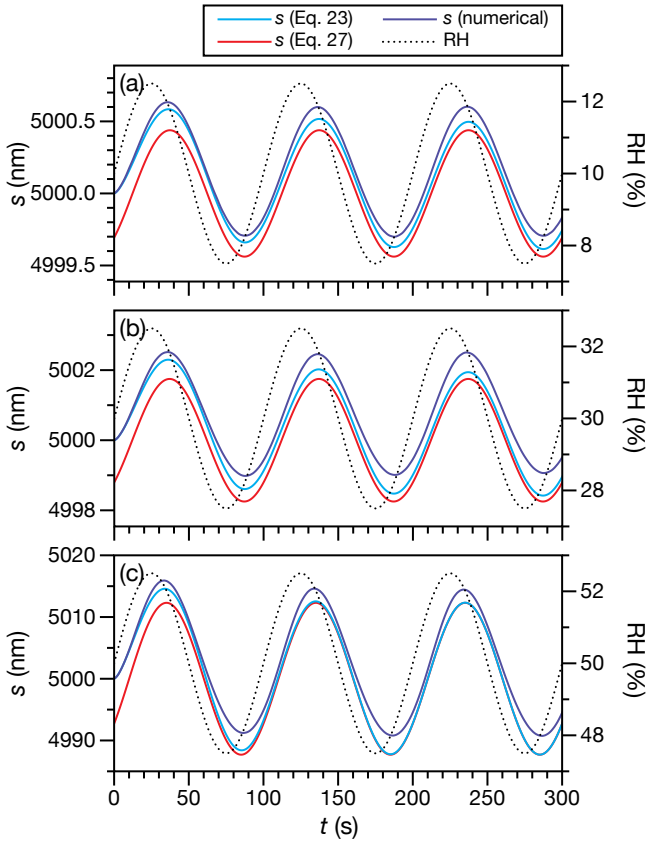

Figure 3: Comparison between the radius, s, calculated analytically using either Eq. 23 or 27 and s calculated numerically for sinusoidal RH oscillations with a period, T, of 100 s and an amplitude of 2.5% at mid-RHs of (a) 10%, (b) 30%, and (c) 50%. The diffusion coefficients at the mid-RHs are (a) 2.92×10^{-16} m^2/s, (b) 2.39×10^{-15} m^2/s, and (c) 6.00×10^{-14} m^2/s. The temperature was set to 298 K and the initial radius, s_0, was 5 μm. Parameters for aqueous sucrose were taken from Ref. 17.

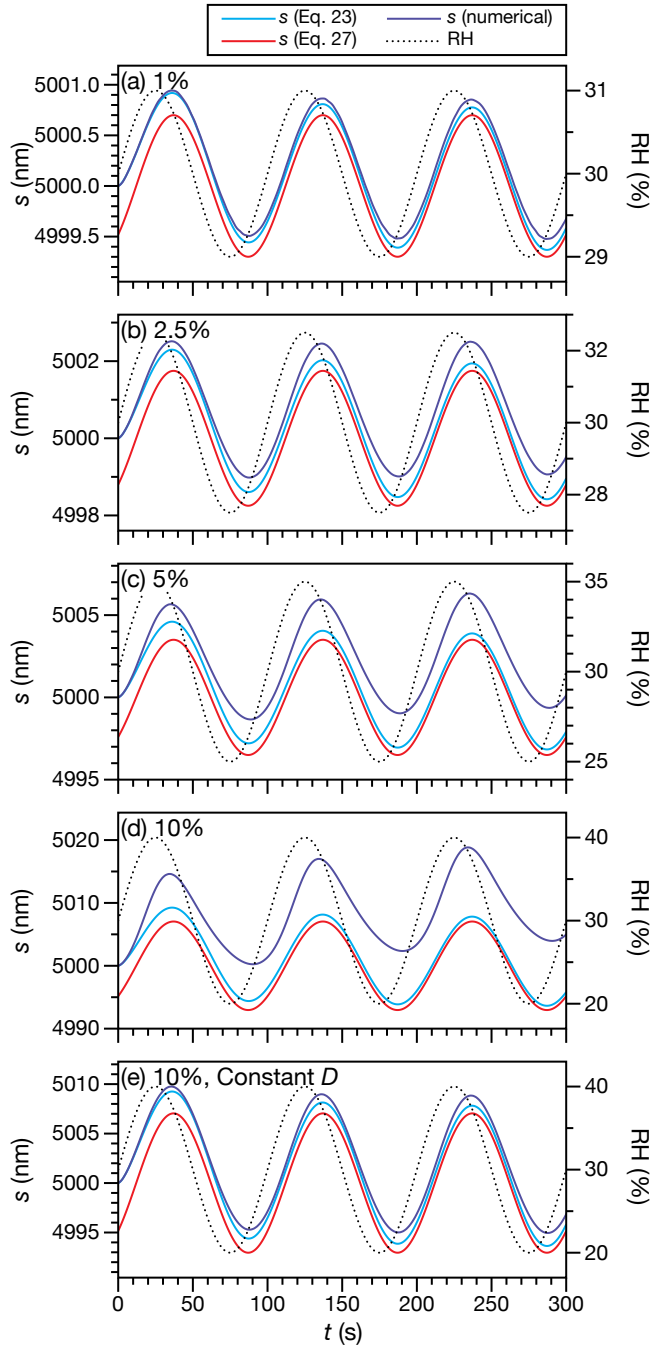

Figure 4: Comparison between the radius, s, calculated analytically using either Eq. 23 or 27 and s calculated numerically for sinusoidal RH oscillations with a period, T, of 100 s and amplitudes of (a) 1%, (b) 2.5%, (c) 5%, and (d) 10% around a mid-RH of 30%. The temperature was set to 298 K and the initial radius, s_0, was 5 μm. Parameters for aqueous sucrose were taken from Ref. 17. All calculations in (e) are identical to (d) except that D does not vary with water activity and is fixed at its value when the RH = 30%.

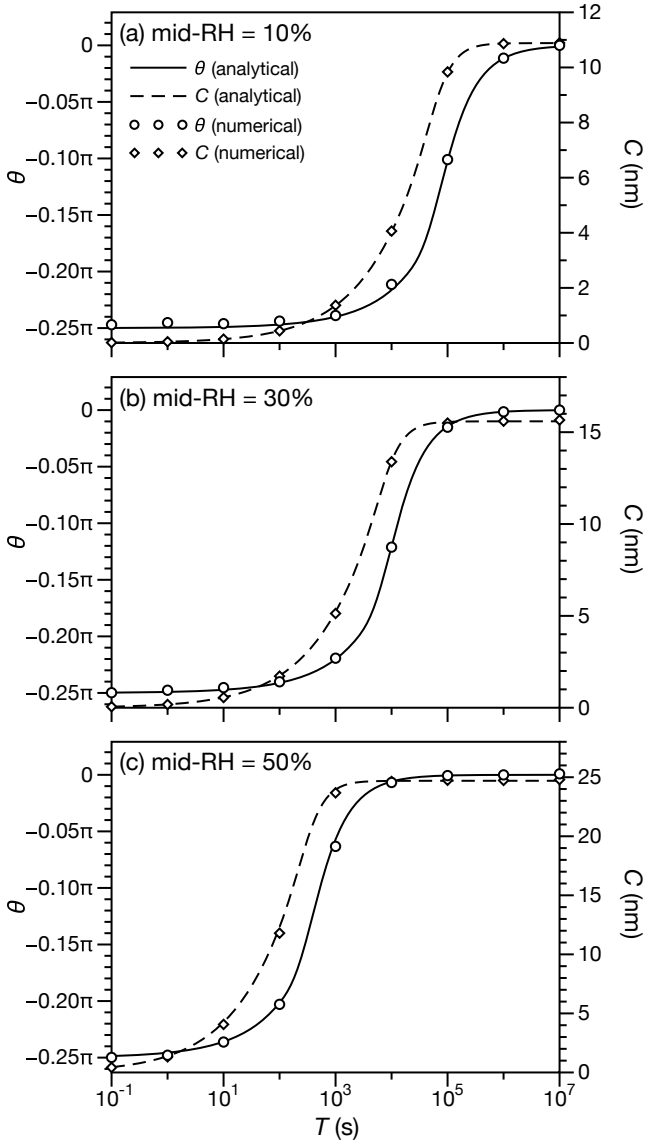

Figure 5: Calculated phase, θ, and amplitude, C, for spherical aqueous sucrose particles as a function of the period, T, of sinusoidal RH oscillations with mid-RHs of (a) 10%, (b) 30%, and (c) 50% with an amplitude of 2.5%. Analytical calculations for θ and C were performed using Eqs. 25 and 24, respectively. Numerical values of θ and C were found by fitting results calculated using the method described in Ref. 17. The temperature was set to 298 K and the initial radius, s_0, was 5 μm. Parameters for aqueous sucrose were taken from Ref. 17.

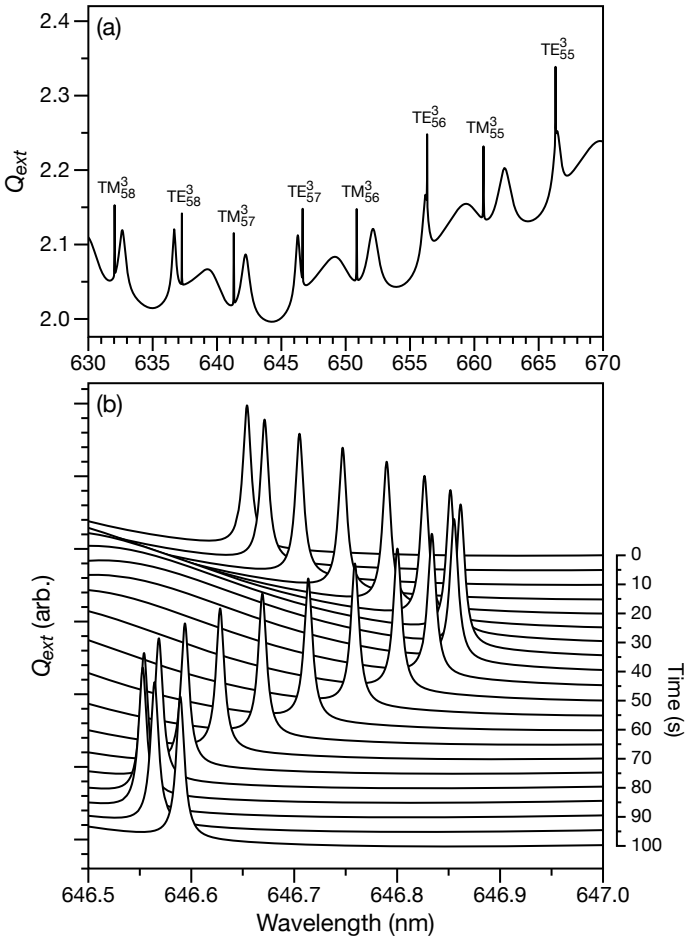

Figure 6: (a) Calculated extinction efficiency, Q_{ext}, for a spherical aqueous sucrose particle equilibrated at RH = 30%. The temperature was set to 298 K and the initial radius, s_0, was 5 μm. All third order modes have been labeled. (b) The TE^3_{57} peak plotted in 5 s intervals during a sinusoidal RH oscillation with a period, T, of 100 s with an amplitude of 2.5%. The traces in (b) have been offset for clarity. Parameters for aqueous sucrose were taken from Ref. 17. Q_{ext} was calculated using the code for electromagnetic scattering from a multilayered sphere (discussed in Ref. 40).

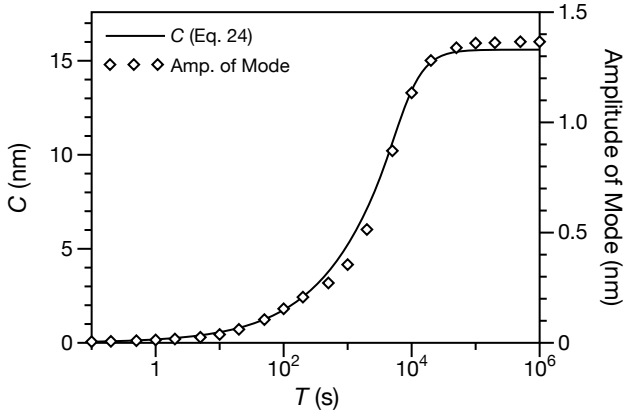

Figure 7: The calculated amplitude of the oscillation in the TE_{57}^{3} mode position for an aqueous sucrose particle in response to RH oscillations across a range of periods, T. This amplitude is superimposed on the amplitude of the oscillation in particle radius, C, that was calculated using Eq. 24. Aside from different values of T, parameters are identical to those listed in the caption of Fig. 6.

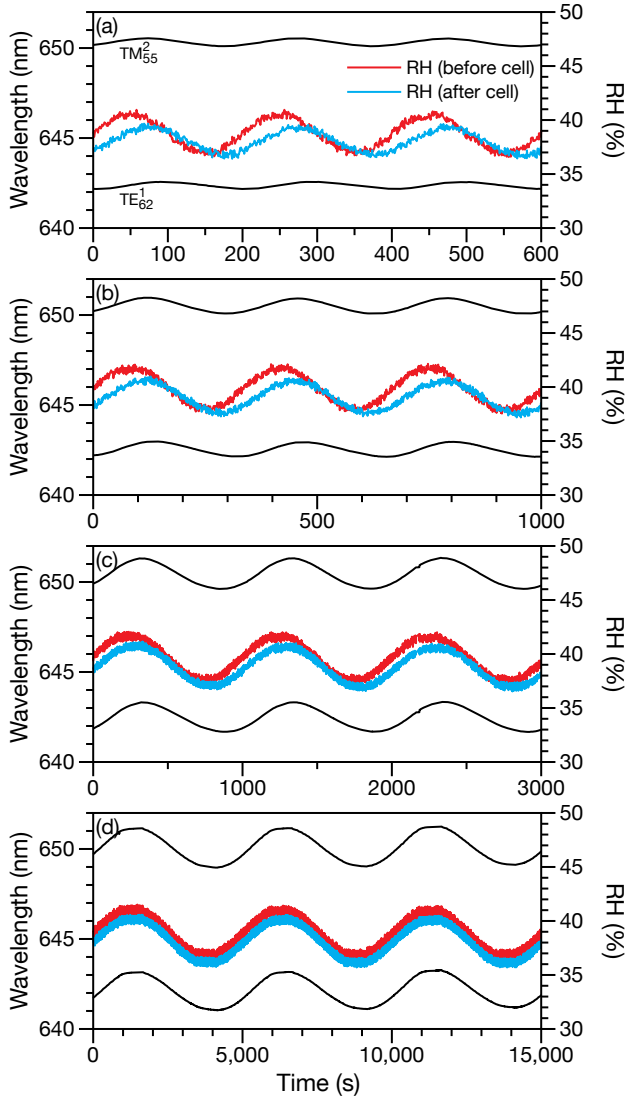

Figure 8: Observed time-dependence of WGM position for the TE^1_{62} and TM^2_{56} modes in an optically trapped aqueous sucrose particle. The RH in the trapping cell oscillates sinusoidally with a period T and amplitude of 2.5% and has a mid-RH of 39%. Measurements of RH were taken before and after the trapping cell and are overlaid on the mode position plots. The values of T are (a) 200 s, (b) 333 s, (c) 1000 s, and (d) 5000 s. Mode positions were extracted from the locations of sharp peaks in cavity-enhanced Raman spectra of the particle. The initial radius of the particle, s_0, was 4630 nm.

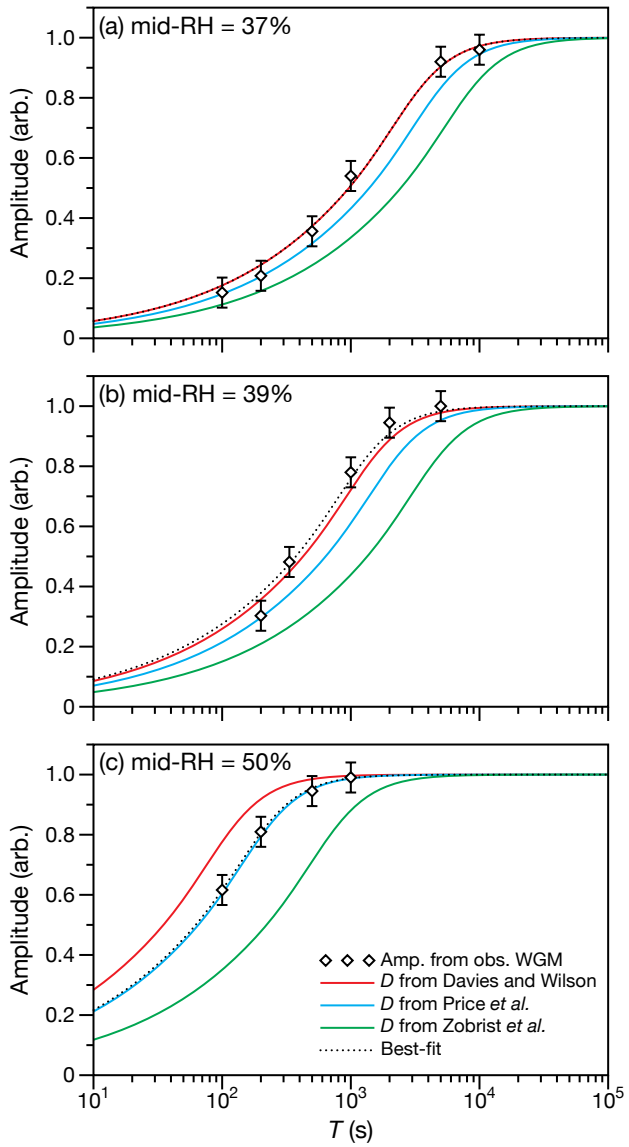

Figure 9: Measured amplitude (arbitrary units) of time-dependent oscillations in one WGM for an aqueous sucrose particle in response to RH oscillations with an amplitude of 2.5% at various periods, T. Particles were held at mid-RHs of (a) 37%, (b) 39%, and (c) 50%. The initial radii, s_0, of the aqueous particles when they were equilibrated at their respective mid-RHs were (a) 5300 nm, (b) 4630 nm and (c) 5000 nm. Solid curves were calculated using Eq. 24 and the parameterizations of the diffusion coefficient, D, from either Davies and Wilson,[31] Price *et al.*,[29] or Zobrist *et al.*[17] The values of D that gave the curves of best-fit were (a) 6.89×10^{-15} m^2/s, (b) 1.36×10^{-14} m^2/s, and (c) 1.01×10^{-13} m^2/s. All measurements and calculations were performed at a temperature of 293 K.

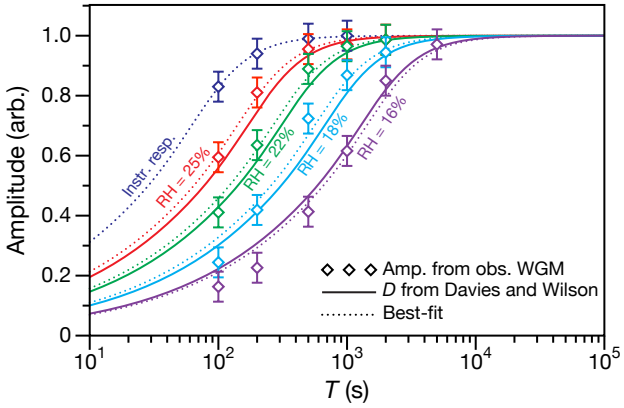

Figure 10: Measured amplitude (arbitrary units) of time-dependent oscillations in one WGM for an aqueous citric acid particle in response to RH oscillations with an amplitude of 2.5% at various periods, T. Particles with initial radii, s_0, of 5500 nm, 5100 nm, 5500 nm, and 5600 nm were held at mid-RHs of 16%, 18%, 22%, and 25%, respectively. Solid curves were calculated using Eq. 24 and the parameterizations of the diffusion coefficient, D, from Ref. 31. Dotted lines are curves of best-fit. The values of D that gave the curves of best-fit (for the listed mid-RH) were 1.10×10^{-14} m^2/s (16%), 2.43×10^{-14} m^2/s (18%), 6.00×10^{-14} m^2/s (22%), and 1.18×10^{-13} m^2/s (25%). All measurements and calculations were performed at a temperature of 293 K.

References

1. S. N. Pandis, R. A. Harley, G. R. Cass and J. H. Seinfeld, *Atmos. Environ.*, 1992, **26A**, 2269-2282.

2. J. F. Pankow, *Atmos. Environ.*, 1994, **28**, 189-193.

3. J. R. Odum, T. Hoffmann, F. Bowman, D. Collins, R. C. Flagan and J. H. Seinfeld, *Environ. Sci. Technol.*, 1996, **30**, 2580-2585.

4. M. Claeys, B. Graham, G. Vas, W. Wang, R. Vermeylen, V. Pashynska, J. Cafmeyer, P. Guyon, M. O. Andreae, P. Artaxo and W. Maenhaut, *Science*, 2004, **303**, 1173-1176.

5. R. Volkamer, J. L. Jimenez, F. San Martini, K. Dzepina, Q. Zhang, D. Salcedo, L. T. Molina, D. R. Worsnop and M. J. Molina, *Geophys. Res. Lett.*, 2006, **33**, L17811.

6. J. H. Kroll and J. H. Seinfeld, *Atmos. Environ.*, 2008, **42**, 3593-3624.

7. M. Hallquist *et al.*, *Atmos. Chem. Phys.*, 2009, **9**, 5155-5236.

8. B. Zobrist, C. Marcolli, D. A. Pedernera and T. Koop, *Atmos. Chem. Phys. Discuss.*, 2008, **8**, 9263-9321.

9. A. Virtanen, J. Joutsensaari, T. Koop, J. Kannosto, P. Yli-Pirilä, J. Leskinen, J. M. Mäkelä, J. K. Holopainen, U. Pöschl, M. Kulmala, D. R. Worsnop and A. Laaksonen, *Nature*, 2010, **467**, 824-827.

10. C. D. Cappa and K. R. Wilson, *Atmos. Chem. Phys.*, 2011, **11**, 1895-1911.

11. M. Shiraiwa, M. Ammann, T. Koop and U. Pöschl, *Proc. Natl. Acad. Sci. USA*, 2011, **108**, 11003-11008.

12. J. H. Seinfeld and S. N. Pandis, *Atmospheric Chemistry and Physics: From Air Pollution to Climate Change*, 3rd ed. John Wiley & Sons, 2016.

13. M. Kuwata and S. T. Martin, *Proc. Natl. Acad. Sci. USA*, 2012, **109**, 17354-17359.

14. L. Renbaum-Wolff, J. W. Grayson, A. P. Bateman, M. Kuwata, M. Sellier, B. J. Murray, J. E. Shilling, S. T. Martin and A. K. Bertram, *Proc. Natl. Acad. Sci. USA*, 2013, 110, 8014-8019.

15. J. F. Davies and K. R. Wilson, *Chem. Sci.*, 2015, **6**, 7020-7027.

16. P. S. J. Lakey, T. Berkemeier, M. Krapf, J. Dommen, S. S. Steimer, L. K. Whalley, T. Ingham, M. T. Baeza-Romero, U. Pöschl, M. Shiraiwa, M. Ammann and D. E. Heard, *Atmos. Chem. Phys.*, 2016, **16**, 13035-13047.

17. B. Zobrist, V. Soonsin, B. P. Luo, U. K. Krieger, C. Marcolli, T. Peter and T. Koop, *Phys. Chem. Chem. Phys.*, 2011, **13**, 3514.

18. D. L. Bones, J. P. Reid, D. M. Lienhard and U. K. Krieger, *Proc. Natl. Acad. Sci. USA*, 2012, **109**, 11613-11618.

19. C. Mund and R. Zellner, *ChemPhysChem*, 2003, **4**, 638-645.

20. B. S. Vaughn, P. J. Tracey and A. J. Trevitt, *Chem. Phys. Lett.*, 2012, **551**, 134-138.

21. U. K. Krieger, C. Marcolli and J. P. Reid, *Chem. Soc. Rev.*, 2012, **41**, 6631-6662.

22. T. C. Preston and J. P. Reid, *J. Opt. Soc. Am. B*, 2013, **30**, 2113-2122.

23. C. Cai, D. J. Stewart, T. C. Preston, J. S. Walker, Y. H. Zhang and J. P. Reid, *Phys. Chem. Chem. Phys.*, 2014, **16**, 3162-3172.

24. B. S. Vaughn, P. J. Tracey and A. J. Trevitt, *RSC Adv.*, 2016, **6**, 60215-60222.

25. M. I. Cotterell, T. C. Preston, A. J. Orr-Ewing and J. P. Reid, *Aerosol Sci. Technol.*, 2016, **50**, 1077-1095.

26. D. M. Lienhard, A. J. Huisman, D. L. Bones, Y.-F. Te, B. P. Luo, U. K. Krieger and J. P. Reid, *Phys. Chem. Chem. Phys.*, 2014, **16**, 16677-16683.

27. A. M. J. Rickards, Y.-C. Song, R. E. H. Miles, T. C. Preston and J. P. Reid, *Phys. Chem. Chem. Phys.*, 2015, **17**, 10059-10073.

28. H. C. Price, J. Mattsson and B. J. Murray, *Phys. Chem. Chem. Phys.*, 2016, **18**, 19207-19216.

29. H. C. Price, B. J. Murray, J. Mattsson, D. O'Sullivan, T. W. Wilson, K. J. Baustian and L. G. Benning, *Atmos. Chem. Phys.*, 2014, **14**, 3817-3830.

30. H. C. Price, J. Mattsson, Y. Zhang, A. K. Bertram, J. F. Davies, J. W. Grayson, S. T. Martin, D. O'Sullivan, J. P. Reid, A. M. J. Rickards and B. J. Murray, *Chem. Sci.*, 2015, **6**, 4876-4883.

31. J. F. Davies and K. R. Wilson, *Anal. Chem.*, 2016, **88**, 2361-2366.

32. A. Moridnejad and T. C. Preston, *J. Phys. Chem. A*, 2016, **120**, 9759-9766.

33. D. M. Lienhard, A. J. Huisman, U. K. Krieger, Y. Rudich, C. Marcolli, B. P. Luo, D. L. Bones, J. P. Reid, A. T. Lambe, M. R. Canagaratna, P. Davidovits, T. B. Onasch, D. R. Worsnop, S. S. Steimer, T. Koop and T. Peter, *Atmos. Chem. Phys.*, 2015, **15**, 13599-13613.

34. R. B. Byrd, W. E. Stewart, E. N. Lightfoot, *Transport Phenomena*, 2nd Ed. John Wiley & Sons, 2007, page 583.

35. J. A. Wesseling and R. Krishna, *Mass Transfer in Multicomponent Mixtures*, Delft University Press, 2000, page 88.

36. S. Alsoy and J. L. Duda, *AIChE J.*, 2002, **9**, 1849-1855.

37. J. W. Lu, A. M. J. Rickards, J. S. Walker, K. J. Knox, R. E. H. Miles, J. P. Reid and R. Signorell, *Phys. Chem. Chem. Phys.*, 2014, **16**, 9819-9830.

38. T. C. Preston and J. P. Reid, *J. Opt. Soc. Am. A*, 2015, **32**, 2210-2217.

39. R. E. H. Miles, J. S. Walker, D. R. Burnham and J. P. Reid, *Phys. Chem. Chem. Phys.*, 2012, **14**, 3037-3047.

40. O. Peña and U. Pal, *Comput. Phys. Commun.*, 2009, **180**, 2348-2354.